Scientia Iranica, Vol. 6, No. 2, pp 112-121

SCIENTIA
IRANICA

Two-Dimensional Temperature Distribution Induced by Various Eelectromagnetic Hyperthermia Applicators

A. Mireshghi* and M. Goharian[1]

Knowledge of temperature distribution resulting from application of a specific probe is an important requirement for an effective hyperthermia treatment plan. Various invasive and non-invasive hyperthermia applicators have been discussed. In order to obtain temperature distribution resulting from these applicators, the Pennes Bioheat Transfer (BHT) equation has been solved using the Finite Element Method (FEM). A single muscle and two other anatomical models have been considered, one being formed by two concentric cylinders of muscle and fat and the other, a rather realistic model consisting of a pelvis containing a tumor. The simple heat transfer model used in the simulation provided reasonable results in all applications that were examined, indicating that the invasive methods, despite of being less popular, are more controllable and flexible in terms of targeting the tumor and avoiding disturbance of the surrounding tissue.

INTRODUCTION

Application of hyperthermia along with other treatment methods, such as radiation and chemotherapy, enhances the effectiveness of cancer treatment through increasing the blood perfusion and oxygenation rate. Various techniques using ultrasonic and electromagnetic waves have been suggested to raise the temperature of a treatment volume to a therapeutic level (~ 41-44°C) for a certain period of time, while keeping the surrounding tissue at a safe, non-toxic temperature [1]. One of the serious problems which has to be overcome before expecting full efficiency from this treatment method is to determine the temperature profile resulting from application of different probes. Temperature measurement in the desired region is restricted by factors such as safety and comfort of the patient. Therefore, development of computer models simulating energy deposition and heat propagation within a biological media can reinforce the applicability of the hyperthermia methods [2]. Electromagnetic energy as a means of heat generation, due to its readiness of transfer, has been the subject of the majority of research work in hyperthermia treatment. In clinical applications, non-invasive methods seem to be preferred, although they suffer from weak tissue temperature control. In the case of invasive methods, since the applicators are implanted in the tumor region, it is much easier to concentrate the generated energy. The most commonly used interstitial applicators are: microwave antennas [3,4], Radio-Frequency (RF) needles [5] and magnetic seeds [6].

In a method where interstitial electrodes are used, a number of stainless steel needles are implanted in the tumor area. The electrodes are then connected to a proper radio-frequency voltage supply. The induced conductive current through the tissue acts as the heat source and raises the temperature in a localized manner. The frequency range of interest in this method is from 0.5 to 13 MHz. The temperature distribution resulting from RF needles is calculated by Strohbehn et al. [7], based on a two-dimensional model.

Microwave probes used in hyperthermia are normally coaxial antennas having diameters of about 1mm with a radiating gap outside the conductor being implanted in the tissue through plastic catheters. The frequency range used by these antennas is usually 300 to 2450 MHz. The possibility of implanting such antennas was first demonstrated by Mendecki et al. [8]. A single antenna radiating at 915 MHz can heat up a

*. *Corresponding Author, Department of Mechanical Engineering, Sharif University of Technology, Tehran, I.R. Iran.*

1. *Department of Mechanical Engineering, Sharif University of Technology, Tehran, I.R. Iran.*

region of about 5 cm along its axis and 2 cm radially. Due to the limited area that can be covered by a single antenna and because most tumors are larger than 2 cm, in practice an array of such antennas must be used. The electric field intensity around a symmetric dipole antenna was calculated based on a model developed by King et al. [9]. Based on this model, Trembly and coworkers [10-12] calculated the SAR resulting from an array of symmetric dipole antennas. The specific absorbed rate was also calculated for an array of asymmetric interstitial dipoles by Zhang et al. [13,14].

In the present work, the goal is to use finite element method to solve the bioheat equation for a variety of source terms in order to find the temperature distribution. A source term is, in fact, the spatial distribution of the Specific Absorption Rate (SAR) resulting from the specific applicator used for hyperthermia treatment. Two different tissue models were considered. One was formed by a two-region cylinder of muscle and fat. The other one was a more realistic model consisting of a pelvis containing a tumor. Here, the results of SAR and temperature distribution calculation in the models are presented after application of plane and cylindrical waves in an external mode hyperthermia. For the interstitial mode, microwave dipole antennas and RF needles have been considered. The temperature distribution is calculated through numerical solution of Pennes bioheat equation [15] using different blood perfusion rates for various tissues.

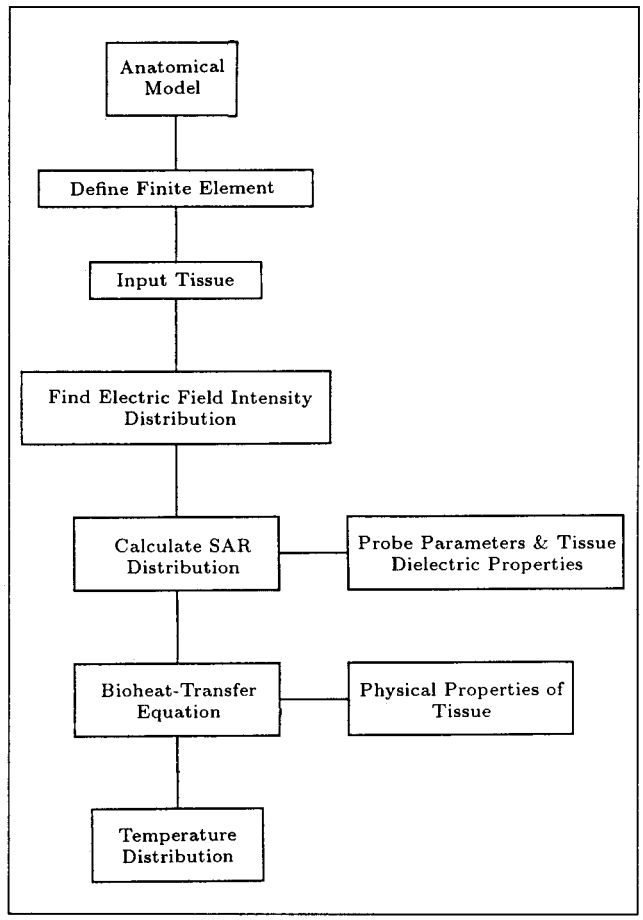

Figure 1. Flow diagram of the sequence of steps in the bioheat-transfer simulation process and temperature distribution calculation.

METHODS

The sequence of steps taken towards reaching the goals of this work namely, calculation of temperature distribution in the tissue region under consideration, are presented in the flow diagram shown in Figure 1. Basic anatomical data about the patient can be obtained using various imaging techniques, normally CT. The key boundary information of the various organs and tissue regions derived from the image is used to create a model which is discretized to form the finite element grid.

In this work, besides plane muscle, two different biological models have been considered; the Fat-Muscle Model (FMM) and the Pelvis Model (PM). The first is a simple two-layer model consisting of coaxial cylinders of muscle and fat tissues. The muscle portion, having a radius of 7.9 cm, is surrounded by a fat region of 15 cm radius. A cross section of FMM is shown in Figure 2a. The second model is the cross section of a pelvis formed by muscle, bone, fat and rectum tissues embedding a tumor, shown in Figure 2b on a 23:100 scale compared to the real dimensions. The finite element grids for these models are shown in Figure 3. More details about the temperature distribution determination procedure using finite element method are presented in the following sections.

Bioheat-Transfer Equation

The temperature profile resulting from the heat generation by various hyperthermia electromagnetic probes, applied to the tissue models, was calculated through solving the Pennes bioheat transfer equation [15]. Substituting the source term with the SAR distribution gives,

$$\rho c \frac{\partial T}{\partial t} = \nabla.(K \nabla T) + \rho_b c_b \omega_b (T_a - T) + \rho(SAR) \ , \quad (1)$$

where:

T = tissue temperature (°C),

ρ = tissue density (kg/m^3),

c = tissue specific heat (W.s/kg°C),

K = thermal conductivity (W/m°C),

ρ_b = blood density (kg/m^3),

c_b = blood specific heat (W.s/kg°C),

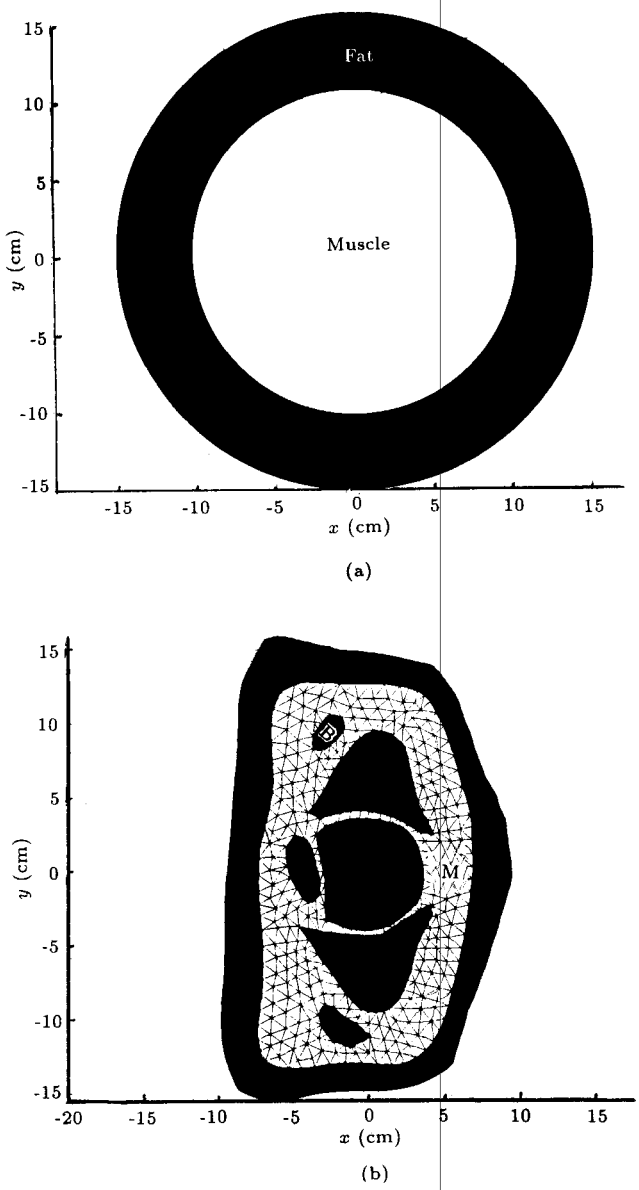

Figure 2. Biological models analyzed; (a) the fat-muscle model, (b) the pelvis model shown on a 23:100 scale.

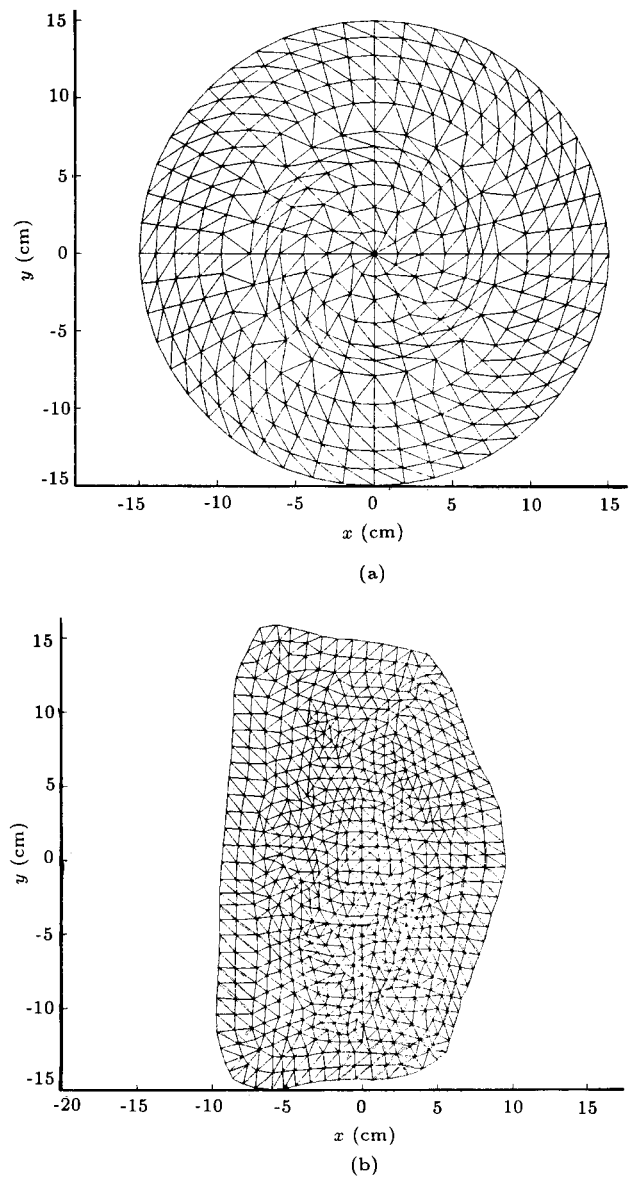

Figure 3. Discretization of the biological models for FEM calculation; (a) the fat-muscle model, (b) the pelvis model.

ω_b = blood perfusion rate (m^3/kg.s),

T_b = temperature of the blood entering the tissue.

In Pennes bioheat model, it is assumed that the energy exchange between blood vessels and the surrounding tissue occurs mainly across the wall of capillaries (vessels with a 5-15 μm diameter). Considering the low blood velocities in capillaries, he assumed that the blood entering the capillary bed has the same temperature as the major supply vessels T_b, but it immediately reaches equilibrium with the surrounding tissue and therefore, leaves the region at the temperature T of the tissue.

There are other bioheat transfer models in the literature such as: Weinbaum and Jiji (WJ) [16] and Chen and Holmes (CH) [17]. In these models, the heat transfer between large arterial and venous vessels and capillaries are taken into consideration. The main problem with the above models is the lack of precise experimental evaluations. Due to the inherent complexity of these models and the requirement for a large number of physiological and geometrical parameters of tissues and vessels involved, the Pennes model was found more practical to use.

Calculation of *SAR*

The rate of energy deposition by electromagnetic waves in tissue is characterized by specific absorption rate (SAR), which is specified in units of Watt per kilogram of tissue and given in terms of the electric field intensity as:

$$SAR = \frac{1}{2}\frac{\sigma}{\rho}|E|^2 \ , \qquad (2)$$

where σ and ρ are conductivity and density of tissue, respectively. A compilation of the electromagnetic properties for biological substances at different frequencies is found in [18].

Saam has calculated the SAR distribution of the biological models of interest for the plane and cylindrical wave [19]. His results have been used in the temperature distribution calculations, however, the obtained temperature values did not reach a therapeutic level in any part of the tissue models. Therefore, it was necessary to recalculate SAR based on the new values of the parameters involved in the electric field intensity distributions. For the case of incidental two-dimensional plane electromagnetic wave with E_z polarization, which is considered here, spatial distribution of the electric field intensity is given by [20]:

$$E_z = E_0 e^{k_0(x\cos\theta + y\sin\theta)} , \tag{3}$$

where E_0 and k_0 denote the amplitude and the wave number, respectively, and θ is the angle of incidence of the plane waves.

Simulation of the incident of cylindrical waves is normally based on a current passing through an infinitely long conductor in the z direction. In this case, the generated electric field propagating as a cylindrical wave in space is given by:

$$E^{inc}(x,y) = \hat{z}E_z,\ E_z = \frac{-\mu_0\omega I_0}{4} H_0^{(2)}(k_0\sqrt{x^2+y^2}) , \tag{4}$$

where:

ω = radiation angular frequency (rad/s),

I_0 = conductor current (A),

μ_0 = permitivity of the medium,

H_0 = Hankle function.

The spatial distribution of the specific absorbed rate for M inserted RF electrodes in a two-dimensional medium is provided as [21]:

$$SAR(x,y) = \frac{\rho/\sigma}{8\pi^2\omega^2|\varepsilon^*|^2} \sum_{i=1}^{M} \frac{I_i[(x-x_i)^2+(y-y_i)^2]}{r_i^2} , \tag{5}$$

where:

σ = the electrical conductivity (mho/m),

ω = angular frequency (rads/sec),

ε^*= complex dielectric constant (farad/m),

I_i = conductor current (amps/m),

x_i = x coordinate of the ith needle,

y_i = y coordinate of the ith needle,

r_i = distance between the point of interest and the ith needle position.

In the case of microwave antennas, for an array of four antennas, considered in this paper, the electric field distribution is given as a function of their x, y and z components and the location of the probes [9]. The components themselves are rather complicated functions of antenna dimensions and the applied voltage V_0, therefore, they have not been repeated here. The SAR distribution is expressed in terms of x, y and z components of the electric field intensities as:

$$SAR = \frac{\sigma}{2\rho}(|E_x|^2 + |E_y|^2 + |E_z|^2) . \tag{6}$$

The resulting SAR distributions were then used in bioheat transfer equation (Equation 1) in order to solve for temperature distribution in the regions of interest.

Finite Element Algorithm

Here, only the steady-state problem $(\frac{\partial T}{\partial t}) = 0$ is considered. It is also convenient to measure temperature relative to the blood temperature T_b. Therefore, the equation of interest would take the following simpler form:

$$\underline{\nabla}.(K\underline{\nabla}T) - \alpha T + \rho S = 0 , \tag{7}$$

where $\alpha = \rho_b c_b \omega_b$ and S is the SAR distribution. The weighted residual statement is obtained through multiplying by an scalar function, φ_i, and integrating over the domain to be modeled:

$$\langle(\underline{\nabla}.K\underline{\nabla}T)\varphi_i\rangle - \langle\alpha T\varphi_i\rangle = -\langle\rho S\varphi_i\rangle . \tag{8}$$

The heat conduction term is integrated by parts, employing the following identity:

$$\langle(\underline{\nabla}.\underline{A})\varphi_i\rangle = -(\underline{A}.\underline{\nabla}\varphi_i) + \int \underline{A}.\underline{n}\varphi_i ds , \tag{9}$$

resulting in:

$$\langle K\underline{\nabla}T.\underline{\nabla}\varphi_i\rangle + \langle\alpha T\varphi_i\rangle = \langle\rho S\varphi_i\rangle + \int K\underline{\nabla}T.n\varphi_i ds . \tag{10}$$

The term $-K\underline{\nabla}T$ in the surface integral is the conduction heat flux across the boundary, which is denoted here as $\underline{q}$. This will result in:

$$\langle K\underline{\nabla}T.\underline{\nabla}\varphi_i\rangle + \langle\alpha T\varphi_i\rangle = \langle\rho S\varphi_i\rangle - \int \underline{q}.\underline{n}\varphi_i ds . \tag{11}$$

The boundary condition for the equation may be written as:

$$\underline{q}.\underline{n} = h(T - T_E) , \tag{12}$$

Table 1. Discretization parameters of the biological models.

Model	*Ne*	*Nn*	PHB	FHB
Fat-Muscle	672	361	72	36
Pelvis	1411	749	561	31

Ne: number of elements of nodes; *Nn*: number of nodes; PHB: primary half bandwidth of coefficient matrix; FHB: final half bandwidth of coefficient matrix.

where h is the heat transfer coefficient and T_E, the ambient temperature of the surrounding. The discretization is completed by expanding the unknown temperature in terms of the weighting function φ_i:

$$T(x,y) = \sum_{j=1}^{N} T_j \varphi_j(x,y) \ . \tag{13}$$

Equation 13 may, then, be enforced for all weighting functions φ_i, $i = 1$ through N, creating N algebraic equations with N unknown T_j.

$$[A]\{T\} = \{b\}, \tag{14}$$

with:

$$A_{ij} = < K \underline{\nabla}\phi_i . \underline{\nabla}\phi_j > + < \alpha \phi_i . \phi_j > + \int h \phi_i \phi_j ds \ . \tag{15}$$

and:

$$b_i = < \rho S \phi_i > + \int h T_E \phi_i ds \ . \tag{16}$$

The equation is then solved with a conventional banded LU decomposition [20].

The discretizations of the biological models (FMM and PM) , necessary for finite element analysis, are shown in Figure 3 and their parameters are given in Table 1. For the complex areas with numerous nodes, the proper numbering of the nodes in the response region can drastically reduce the bandwidth of the matrices. For this purpose, Collins model has been used [22]. Furthermore, the formulation of the boundary values is based on Ritz method [20] and the boundary condition given in Equation 12 is also used.

SIMULATION RESULTS

One of the non-invasive methods of hyperthermia simulated in this work is the plane electromagnetic wave. SAR and temperature distribution resulting from the radiation of plane waves have been calculated at $\theta = 0$ degree (parallel to x-axis) on the FMM. Both distributions (Figure 4) show the expected asymmetry due to $1/r^2$ fall of amplitude in the model. The

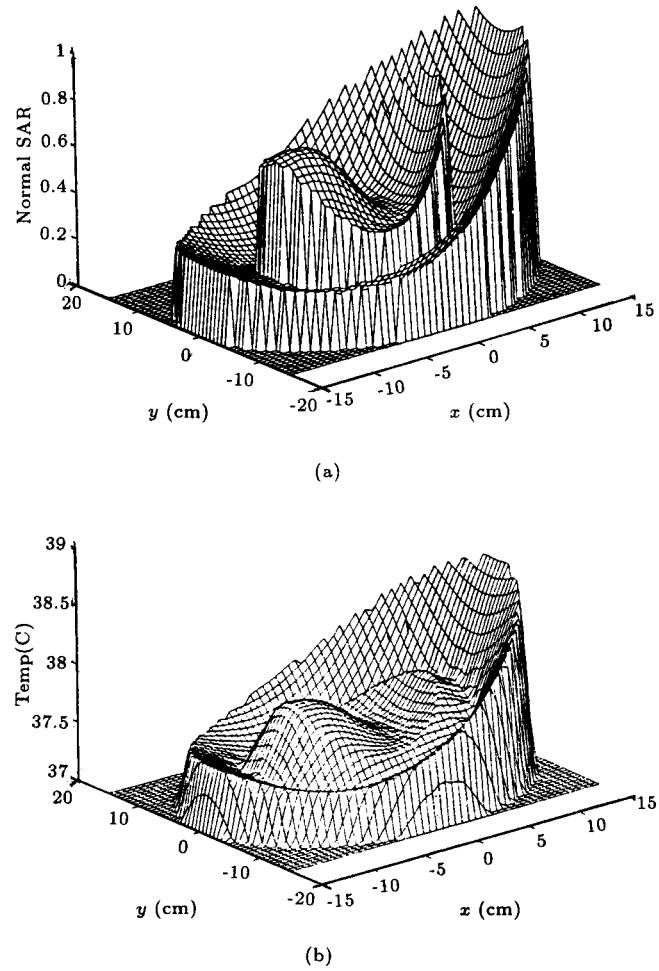

Figure 4. The simulation results from a plane wave radiated at $\theta = 0°$ on the fat-muscle model, (a) SAR and (b) temperature distribution.

illustrated temperature variation closely follows the SAR distribution. The blood perfusion rates in the muscle and fat tissues are assumed to be 16 and 5 ml/min per 100 grams. The effect of different values of σ/ρ for fat and muscle are quite visible in the SAR distribution. The temperature distribution also shows the effects of higher perfusion rate and conductivity in the muscle region. Temperature variations in the pelvis model resulting from plane waves at 0 and 180 degrees also demonstrate a very good agreement with their associated SAR distributions. The value of the perfusion rates used for various tissues in the pelvis model are given in Table 2. SAR and the temperature distributions resulting from application of cylindrical waves are presented in Figure 5. SAR and temperature distribution in Figures 5a and 5b were calculated with

Table 2. Perfusion rates used for tissues forming the pelvis model.

Muscle	Fat	Bone	Tumor	Rectum
16	5	0	10	12

$I_0 = 6A$ at 100 MHz. Electromagnetic and thermal characteristics of some tissue at this frequency are given in Table 3. As one can see from Figure 5, at $I_0 = 6$A, although the temperature rise is more pronounced in the tumor region, it does not reach a therapeutic level. Increasing the current value raised the temperature in the bone region more than in the tumor (see Figure 6 for $I_0 = 9$A). These results indicate that the external plane and cylindrical waves are not effective for non-superficial treatments, because they can not deliver energy in a selective manner to a specific internal region

Table 3. Electromagnetic and thermal characteristics of some tissues at 100 MHz.

Tissue	ε_r	μ_r	σ	K	ρ_c
(M)	72	1	0.89	0.64	3.7× 106
(F)	10.5	1	0.22	0.21	2.12 × 106
(B)	10	1	0.02	0.43	2.23 × 106
(T)	72	1	0.89	0.64	3.7×106
(R)	52	1	0.61	0.54	3.9×106

M, F, B, T and R stand for: muscle, fat, bone, tumor and rectum tissues, respectively.

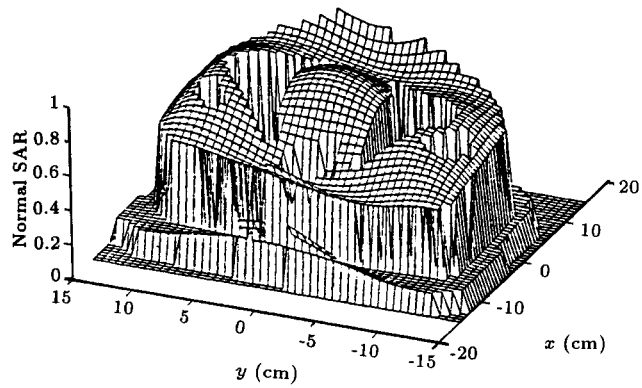

(a)

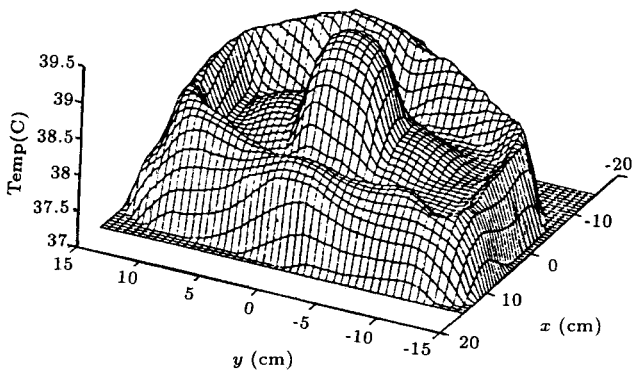

(b)

Figure 5. The SAR (a) and the temperature (b) distributions resulting from cylindrical waves radiated on the pelvis model ($I = 6$ A).

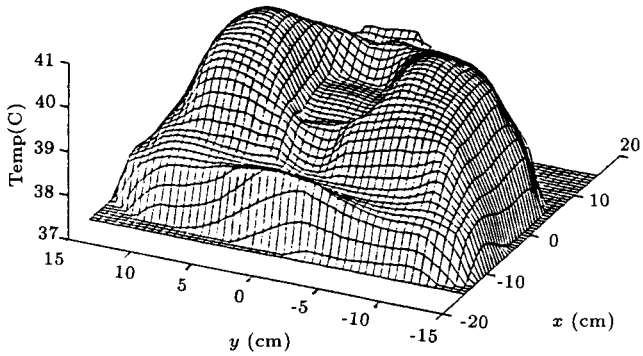

Figure 6. The temperature distributions resulting from cylindrical waves radiated on the pelvis model ($I = 9$ A).

such as a tumor, without damaging the surrounding tissue.

For evaluating the invasive methods, first the results from the simulation of implanted RF needles in a muscle region are discussed. The temperature distribution resulting from a needle inserted at $x = 1$cm and $y = 0$ excited with a current of 6A at RF frequency of 13 MHz is shown in Figure 7. The therapeutic temperatures (≥ 42°C) seem to occur at radii smaller than 1.9 cm. This is called "therapeutic radius" and hereafter is denoted by R_t. Furthermore, the effect of variation of both excitation current and frequency on the peak temperature (T_p) and R_t of a single RF needle are studied. The results are shown in Figures 8 and 9. At the simulated RF frequency of 13 MHz, the peak temperature T_p rises with an increasing slope, while the therapeutic temperature R_t rises with a declining slope and tends to saturate at about 10A. It is interesting to note both R_t and T_p variations with RF frequency peak at 8 MHz. When two needles are implanted, due to accumulative effect in the distance between them, one expects the therapeutic temperature at the needles separation to hold values somewhat greater than $2R_t$. In fact, the simulation proved this to be true as seen in

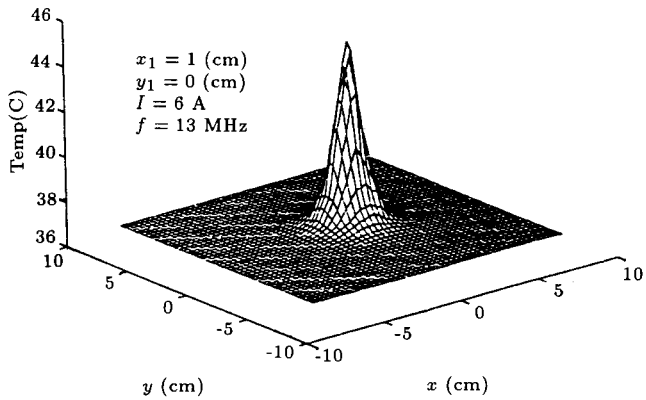

Figure 7. The temperature distribution resulting from implanting a RF needle with 6 A at $x = 1$cm and $y = 0$ in a single muscle region.

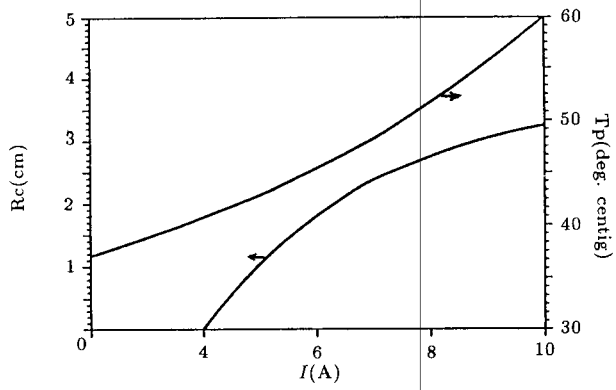

Figure 8. Variation of the therapeutic radius (R_t) and peak temperature (T_p) versus needle excitation current.

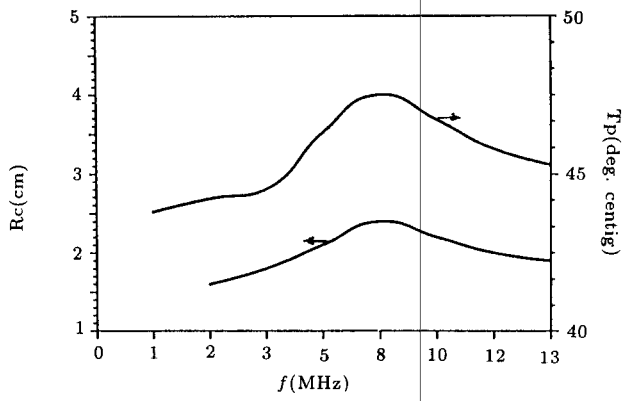

Figure 9. Variation of the therapeutic radius (R_t) and peak temperature (T_p) versus needle excitation frequency.

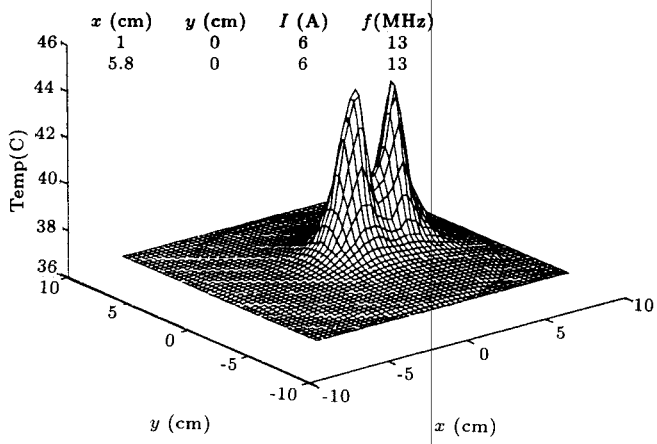

Figure 10. The temperature distribution resulting from two RF needles excited at 13 MHz and with current of 6 A implanted in a single muscle tissue.

the limiting case shown in Figure 10. The separation between needles in that figure is 4.8 cm, which is about 25% larger than $2R_t$. In Figure 11, the temperature distribution resulting from implanting four RF needles in the tumor region of the pelvis model is presented. The locations and the currents are shown in the figure, in which several interesting features are observed:

a) Due to the small needle distance in the y direction

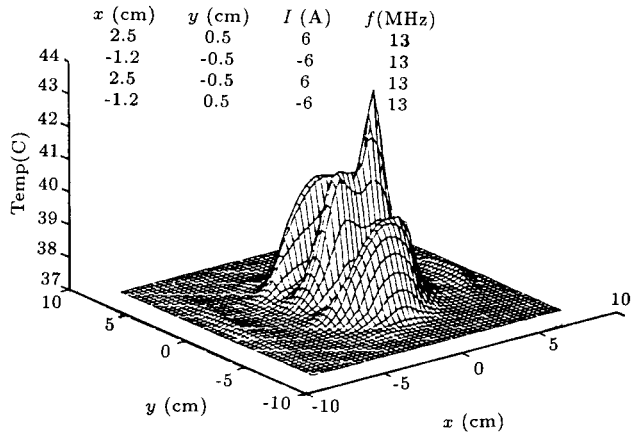

Figure 11. The temperature distribution resulting from four RF needles excited at 13 MHz implanted in the tumor region of the pelvis model. The location of the needles and their excitation currents are given in the figure.

(1 cm), the two peaks are merged together in that direction.

b) The temperature rise at the needles in the vicinity of the rectum region is less due to the higher perfusion rate in that tissue compared to the muscle tissue in the right hand side of the tumor.

c) Due to lower heat transfer coefficient and zero perfusion rate in the bone region (top and bottom parts), pronounced temperature rise is observed in that region. All these facts support the validity of the simulation and the applied heat transfer model.

To simulate the application of microwave probes, an array of four antennas with characteristics shown in Table 4 (also see Figure 12) were considered, implanted 4 cm apart on the corners of an square. Again, first a simple tissue model consisting of a single muscle region was considered. The resulting temperature profile, with two antennas having phase angles of π ($\theta_1 = \pi$, $\theta_2 = 0$, $\theta_3 = 0$, $\theta_4 = \pi$) is shown in Figure 13. Simulation of the same array of antennas (with phase angles of 0) implanted in the FMM demonstrated a flatter top but narrower central peak in the muscle region and a smaller one in the peripheral section (Figure 14), again a consequence of weaker heat transfer in the fat tissue. As expected, the change of phase has shown its controlling effect on the peak temperature and the therapeutic temperature region. In the analysis of the pelvis model, the distance between the antennas in the array, implanted in the tumor region, was changed to 2 cm. For the case in which all antennas were assumed to be in phase with each other, the temperature peaked in the center of the array with no significant increase in

Table 4. Characteristics of the microwave antenna.

f(MHz)	ε_2	ε_3	V_0	h_1	h_2	a	b	c
915	1	2.55	1	1.9089	13	0.475	0.684	1.019

V_0 in Volts; h_1 and h_2 in cm; and a, b and c in mm.

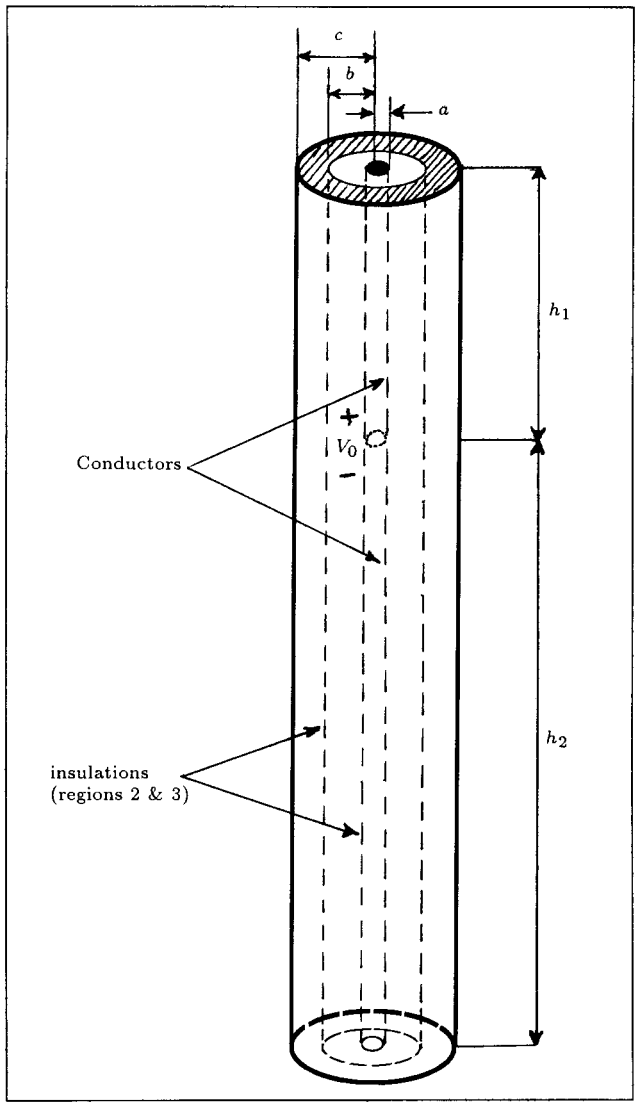

Figure 12. Schematic structure of one of the microwave antennas used. The values of parameters are given in Table 4.

the surrounding tissue, except for a small rise observed in the fat ring (see Figure 15). For this model, also, the temperature profile could be manipulated through varying the phase of different antennas. This effect is shown in Figures 16 and 17, for ($\theta_1 = \pi$, $\theta_2 = 0$, $\theta_3 = 0$, $\theta_4 = \pi$) and ($\theta_1 = \pi$, $\theta_2 = 0$, $\theta_3 = \pi$, $\theta_4 = 0$), respectively.

CONCLUSION

In this paper, after assessing various invasive and non-invasive hyperthermia methods based on electromagnetic radiation, the temperature distributions resulting from various electromagnetic hyperthermia applicators were analyzed by numerically solving the Pennes bio-heat equation in three biological models, using finite element method. The knowledge of such temperature profiles provided by simulation methods is expected

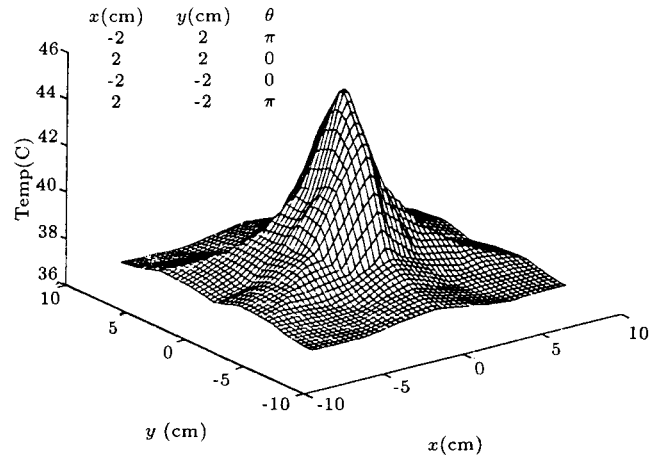

Figure 13. The temperature profile resulting from the implantation of an array of four microwave antennas with $\theta_1 = \pi$, $\theta_2 = 0$, $\theta_3 = 0$ and $\theta_4 = \pi$ implanted in a single muscle region.

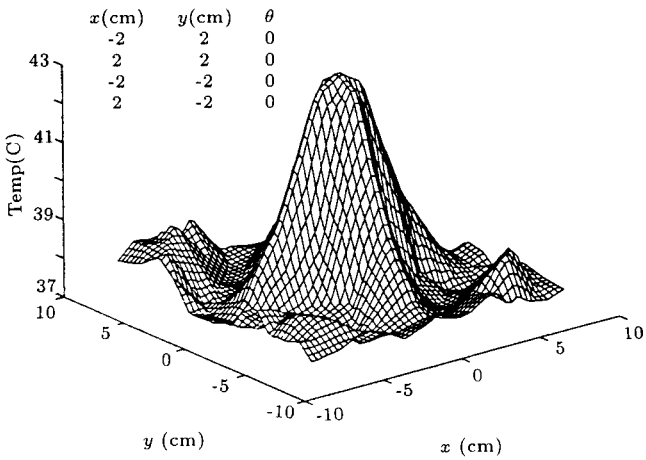

Figure 14. The temperature distribution resulting from the implantation of an array of four equal phase microwave antennas implanted in fat-muscle model.

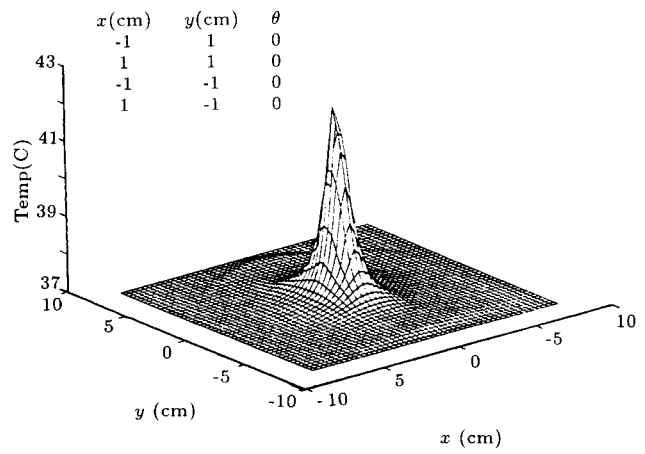

Figure 15. The temperature profile resulting from the implantation of an array of four equal phase microwave antennas (spaced two cm apart) implanted in the tumor region of the pelvis model.

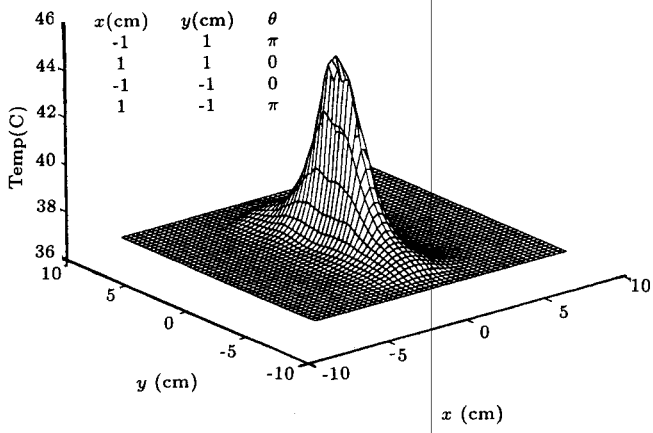

Figure 16. The temperature profile resulting from the implantation of an array of four microwave antennas (spaced two cm apart) with $\theta_1 = \pi$, $\theta_2 = 0$, $\theta_3 = 0$ and $\theta_4 = \pi$ implanted in the tumor region of the pelvis model.

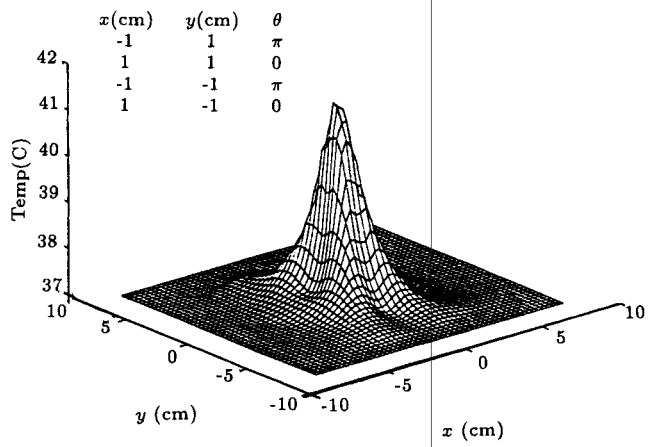

Figure 17. The temperature profile resulting from the implantation of an array of four microwave antennas (spaced two cm apart) with $\theta_1 = \pi$, $\theta_2 = 0$, $\theta_3 = \pi$, and $\theta_4 = 0$ implanted in the tumor region of the pelvis model.

to enhance the effectiveness of hyperthermia methods in cancer treatment. The simulation results presented here indicate that the non-invasive methods (plane and cylindrical waves) are not effective for non-superficial treatments, because they cannot deliver energy in a selective manner to a specific internal region such as a tumor, without damaging the surrounding tissue. For RF needles, the dependency of the peak temperature and the therapeutic radius on the excitation current and frequency were studied. For arrays of microwave antennas, the expected effect of phase variation on changing the temperature distribution was observed. Although there were not any available experimental data to compare with the obtained results, it can be concluded that the simple heat transfer model used in the simulation provided reasonable results in all applications that were considered here.

ACKNOWLEDGMENT

The authors would like to express their thanks to Mr. S. Saam for his valuable help in the numerical and computer programming part of this research.

REFERENCES

1. Strohbehn, J.W. and Douple, E.B. " Hyperthermia and cancer therapy: A review of bimedical contributions and challenges", *IEEE Trans. Biomed. Eng.*, **31**(1), pp 779-787 (1984).
2. Strohbehn, J.W. and Roemer, R.B. "A survey of computer simulations of hyperthermia treatment", *IEEE Trans. Biomed. Eng.*, **31**(1), pp 136-149 (1984).
3. Strohbehn, J.W., Bowers, E.D., Walsh, J.E. and Douple, E.B. " An invasive microwave antenna for locally-induced hyperthermia for cancer therapy", *J. Microwave Power*, **14**, pp 339-350 (1979).
4. Lyon, B.E., Birth, R.H. and Strohbehn, J.W. " Localized hyperthermia, in the treatment of malignant brain tumors using an interstitial microwave antenna array", *IEEE Trans. Biomed. Eng.*, **BE-31**(1), pp 53-62 (1984).
5. Astrakhan, M.A. and Norman, A. "A localized current field hyperthermia system for use with 192-iridium interstitial implants", *Med. Phys.*, **9**, pp 419-424 (1982).
6. Stouffer, P.R., Caters, T.C., Fetter, A.M., Deign, D.W., Dewiest, M.W., Oleos, J.R. and Roomer, R.B. "Observations on the use of ferromagnetic implants for inducing hyperthermia", *IEEE Trans. Biomed. Eng.*, , **BME-31**(1), pp 76-96 (1984).
7. Strohbehn, J.W. and Roemer, R.B. "Temperature distributions from interstitial rf electrodes hyperthermia system; theoretical predictions", *Int. J. Radiat. Oncol. Biol. Phys.*, **9**, pp 1655-1667 (1983).
8. Mendecki, J. et al. "Microwave applicators for localized hyperthermia treatment of malignant tumors", *J. Biomed., Eng.*, **1**, pp 511-518 (1977).
9. King, R.W.P., Trembly, B.S. and Strohbehn, J.W. "The electromagnetic field of an insulated antenna in a conduction or dielectric medium", *IEEE Trans. Microwave Theory Tech.*, **MTT-31**, pp 574-583 (July, 1983).
10. Trembly, B.S. "The effect of driving frequency and antenna length on power deposition within a microwave antenna array used for hyperthermia", *IEEE Trans. Biomed. Eng.*, **BME-32**(1), pp 152-157 (1985).
11. Trembly, B.S. et al. "Control of SAR pattern within a microwave antenna array through variation of antenna driving phase", *IEEE Trans. Microwave Theory Tech.*, **MTT-34**, pp 568-571 (May, 1986).
12. Trembly, B.S., Wilson, A.H., Harvard, J.M., Sabatakaksi, K. and Strohbehn, J.W. "Comparison of power deposition by in-phase 433 MHz and phase-modulated 915 MHz interstitial antenna array hyperthermia", *IEEE Trans. Microwave Theory Tech.*, **MTT-36**, pp 908-916 (May, 1988).

13. Zhang, Y., Dubal, N.Y., Hambleton, R.T. and Joines, W. "Determination of the electromagnetic field and SAR pattern of an interstitial applicator in a dissipative dielectric medium", *IEEE Trans. Microwave Theory Tech.*, **36**(10), pp 1438-1443 (Oct., 1988).

14. Zhang, Y., Joines , W. and Oleson, J.R. "The calculated and measured temperature distribution from a phased interstitial antenna array", *IEEE Trans. Microwave Theory Tech.*, **38**(1), pp 69-76 (Jan. 1990).

15. Pennes, H.H. "Analysis of tissue and arterial blood temperature in resting forearms", *J. Appl. Physiol.*, **1**, pp 93-122 (1948).

16. Weinbaum, S. and Jiji, L.M., "A new simplified bioheat equation for the effect of blood flow on local average tissue temperature", *ASME J. Biomech. Eng.*, **207**, pp 131-139 (1985).

17. Chen, M.M. and Holmes, "Microvascular contributions in tissue heat transfer", *Annals of the New York Academy of Sciences*, **335**, pp 137-150 (1980).

18. Stuchly, M.A. and Stuchly, S.S. "Dielectric properties of biological substances-tabulated", *Journal of Microwave Power*, **15**(1) (1980).

19. Saam, S. "Evaluation of specific absorbed rate from electromagnetic waves in biological tissues using finite element method", MSc. Thesis, Sharif University of Technology, Tehran, Iran (April, 1997).

20. Jin, J., *The Finite Element Method in Electromagnetics*, John Wiley & Sons (1993).

21. Goharian, M. "Assessment of hyperthermia methods based on electromagnetic wave generators and evaluation of temperature distribution", MSc. Thesis, Sharif University of Technology, Tehran, Iran (Jan., 1998).

22. Collins, R.J. "Bandwidth reduction by automatic renumbering", *Int. J. Num. Meth. Eng.*, **6**, pp 345-356 (1973).